国际化材料实验教学的探索

上海交通大学材料科学与工程
周伟敏

01 材料实验教学中心概况

02 国际化实验教学介绍

03 赛事展望

学院在校生约为1500人，
本科生约560人，硕士研究生约470人，博士研究生约360人

培养模式

确立“双轮驱动”的分类培养模式

本科人才培养模式

徐祖耀荣誉班（国际班）

平行班

卓越工程师班

实验教学中心

实验教学中心

整体情况：独立本科教学实验中心

场地建设：面积达800 m^2

经费支持：近三年共计投入约1200 万

配备师资：固定人员23 名，其中专职教师3名

2019获批上海市实验教学中

化学合成实验室

生物材料实验室

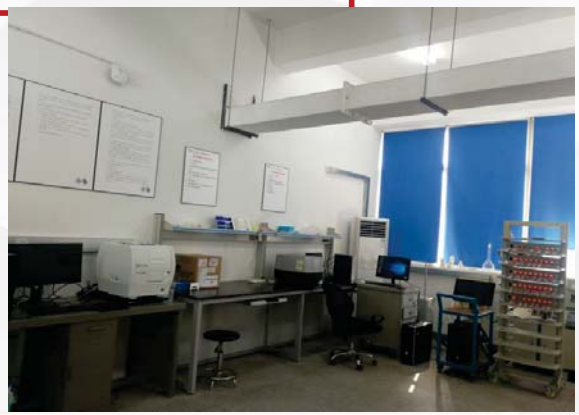

高分子材料实验室

人才培养

上海交通大學 SHANGHAI JIAO TONG UNIVERSITY

构建了多层次、多维度实验实践教学体系

- 近4年学生共计获成果112项
  - 市级及以上大学生创新项目18项
  - 市级及以上奖励56项
  - 科研论文24篇
  - 专利14项
- 获上海本科重点教改项目立项

人才培养


实验教学中心的工作
本科生培养
研究生培养
材料学院
交大-密西根联合学院
交大-巴黎高科卓越工程师学院
交大致远学院
培养研究生（720余人次）
提供测试服务（2000余人次）

2020年开设的综合实验：

- 1、原位自生高性能TiB2/7075铝基复合材料
- 2、合金钢的过冷奥氏体转变曲线（CCT）的测试
- 3、低碳钢焊接试验设计与分析
- 4、铝钢异种材料焊接组织与性能分析
- 5、钢钛异种材料焊接组织与性能分析
- 6、FeCoNi三元相图的测试分析
- 7、镍钛合金形状记忆效应的应用
- 8、可降解医用材料（镁、锌合金）的体外降解研究实验
- 9、红外成像在热处理中应用
- 10、高分子材料性能评价
- 11、钙钛矿量子点的合成与表征
- 12、荧光微纳米球在生物检测上的应用研究
- 13、碳基单原子氧还原电催化材料的制备和应用

01 材料实验教学中心概况

02 国际化实验教学介绍

03 赛事展望

材料实验教学国际班简介

2016年，材料学院开设国际班，专业课全英语教学

2017年秋季，首次实验教学采用英语教学，学生数24人

国际化实验课程的目标

Undergraduate Program for the International Education

Experimental Class of SMSE@SJTU

Mission

To provide internationally recognized education in the field of materials science and engineering, cultivating students with strong problem solving abilities in science and engineering, global vision, as well as communication and teamwork skills.

Objectives

The International Program aims to cultivate students capable of:

- Solving complex science engineering problems by making use of their understanding of the relationships of microstructure, properties, performance, and processing of materials.
- Perceiving and following the rapidly changing scientific and technological trends, and driving the development of future technologies.
- Communicating effectively with colleagues or peers all over the world.
- Making substantial contribution to science, technology, and society.

具体实施方法

第一次上课安全教育、介绍报告撰写方式（参照论文格式）

实验报告以小组方式提交，对学生的实验报告进行讲解

定期组织口头汇报

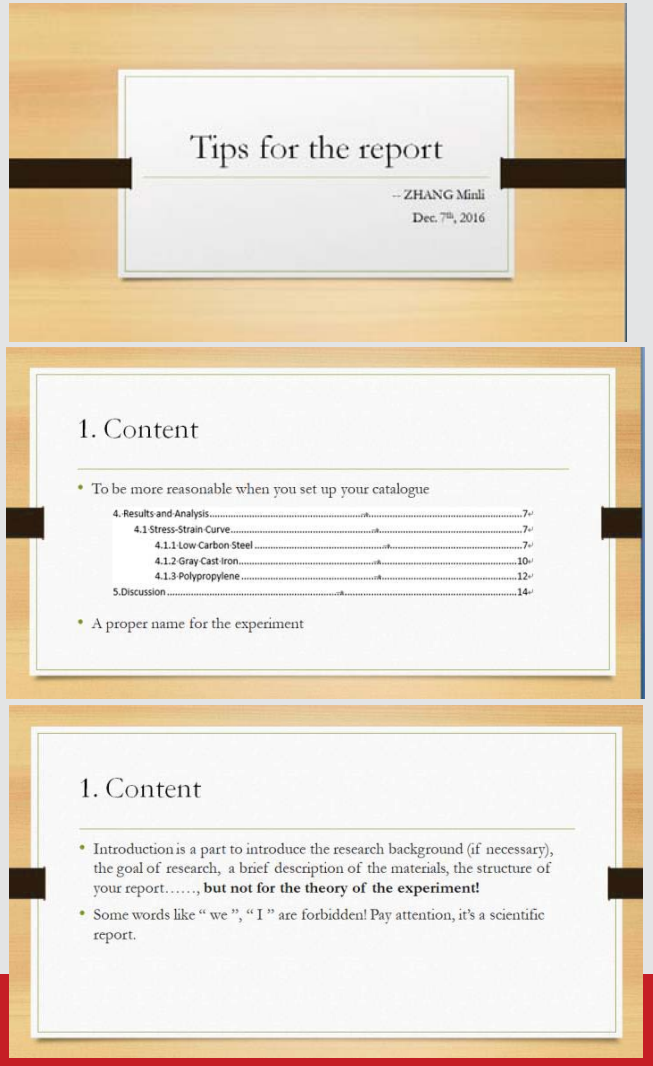

案例1 材料拉伸实验（14级学生-首届）

Tensile test and fracture morphology analysis

By Miguang Sun（5140519014）
Guided by Weimin Zhou, Xueyan Wu

A report submitted in partial fulfillment of
the requirements for
MT344 Materials Lab I course

School of Materials Science and Engineering
3 November 2016

ABSTRACT

Tensile testing is a basic material science method to measure material properties, several mechanical properties are directly measured via a tensile test, such as yield strength, maximum elongation and reduction in area for ductile materials and ultimate strength for both ductile and brittle materials. Based on measurements, Young's modulus, Poisson's ratio, toughness etc. can be derived. Especially, uniaxial tensile testing is the most common and convenient for obtaining the mechanical characteristics of isotropic materials. Fracture morphology characterization is another significant method to determine the properties of materials since different properties correspond to completely morphology of fracture, since fracture morphology records all the information loyally from the initiation of crack to propagation of crack till final fracture. By using field emission scanning electron microscopy (SEM) with its magnification from 40 to 1000, to characterize the facture surface, more mechanical properties of materials and mechanisms of fracture for different materials are revealed.

LIST OF TABLES

LIST OF FIGURES

TABLE OF CONTENTS

案例1 材料拉伸实验

INTRODUCTION

Tensile testing, also known as tension testing is a fundamental materials science test in which a sample is subjected to a controlled tension until failure. Properties that are directly measured via a tensile test are ultimate tensile strength, maximum elongation and reduction in area. From these measurements the following properties can also be determined: Young's modulus, Poisson's ratio, yield strength, and strain hardening characteristics. Uniaxial tensile testing is the most commonly used for obtaining the mechanical characteristics of isotropic materials.

Fracture morphology characterization is another significant method to determine the properties of materials since different properties correspond to completely morphology of fracture. Scanning electron microscopy is a widely accepted tool for fracture morphology analysis for the convenient specimen preparation, continuous magnification and high stereoscopic sense, etc. With the help of scanning electron microscopy (SEM), direct observation and analysis of the macroscopic and microscopic structure of fracture surface, fracture morphology records all the information loyally from the initiation of crack to propagation of crack till final fracture. In the experiment, magnification range is from 40 to 1000. In the low magnification, the initial position and the crack growth path can be judged by the macroscopic observation. In that case, more mechanical properties of materials are revealed. Whereas, in the high magnification, analysis of the causes and mechanisms of fracture can be adopted.

THEORY

1. Tensile testing and mechanical parameters

1.1. Tensile testing

Tensile testing is a fundamental method to measure the mechanical properties in the field of material. While testing, both ends of sample are gripped by fixtures and the sample is subjected to a controlled tension till fracture. Basically, uniaxial tensile testing is used for obtaining the mechanical characteristics of isotropic materials, meanwhile, the testing system can provide a stress-strain curve automatically recording and depicting material mechanical properties. A quintessential stress-strain curve for ductile material is shown in Fig.1. Brittle material's stress-strain curve will be different but much simpler than ductile one.

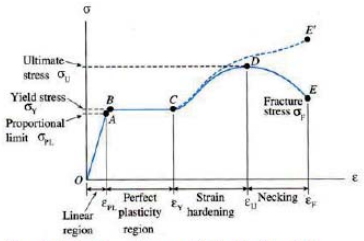

Figure 1 A typical stress-strain curve for ideal ductile materials

1.2. Mechanical parameters

During tensile testing, properties like ultimate tensile strength, maximum elongation and reduction in area can be directly measured. A stress-strain curve can be used to obtain other properties: Young's modulus, Poisson's ratio, yield strength, and strain hardening characteristics, simultaneously. Corresponding formulas for calculating the quantities are shown below:

$$E=\frac{\sigma}{\varepsilon}=\frac{\nabla\sigma}{\nabla\varepsilon}=\frac{\nabla F/S_0}{\nabla l/l_0}=\frac{\nabla F\cdot l_0}{\nabla l\cdot S_0}(N/mm^2)$$

$$R_{P0.2}=\frac{F_{P0.2}}{S_0}(N/mm^2);\mathrm{Re}_{eH}=\frac{F_{eH}}{S_0}(N/mm^2);$$

$$\mathrm{Re}_{eL}=\frac{F_{eL}}{S_0}(N/mm^2);R_m=\frac{F_m}{S_0}(N/mm^2);$$

$$A=\frac{\nabla lu}{l_0}=\frac{lu-l_0}{l_0}\times100\%;Z=\frac{S_0-Su}{S_0}\times100\%$$

2. Fracture morphology

Fracture is the separation or fragmentation of solids into two or more pieces under the action of stress. Generally speaking, any fracture includes two steps—crack formation and propagation— in response to an imposed stress, meanwhile, propagation can be subdivide into slow propagation and rapid propagation which will give rise to completely different fracture morphology. From macroscopic aspect, fracture can be treated as two types: brittle and ductile.(shown in Fig.2)

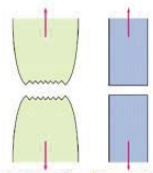

Figure 2 Two typical profiles of macroscopic fracture [1]

Based on fractography, the fracture morphology can be divided into different categories according to different criteria, it can be list as shown in Tab.1

Table 1 Types of fracture based on different criteria[2]

Criteria	Categories	Schematic graph
Amount of deformation prior to fracture	(a)Brittle (b)Ductile	
Orientation between normal stress and fracture surface	(c)Orthogonal (d)Shear	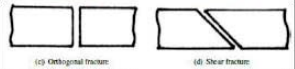
Crack propagation path	(e)Intergranular (f)Transgranular	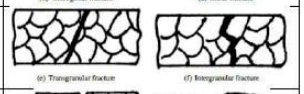
Fracture mechanism	(g)Cleavage (h)micro-voids coalescence (i)pure shear	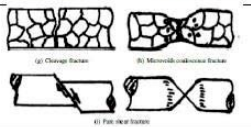

EXPERIMENTAL DETAILS

1. Materials:

Table 2 Material and its related parameters

MATERIAL	STANDARD	TYPE	PARAMETERS

案例1 材料拉伸实验

Low carbon steel (Fe-0.2wt%C)	GB/T 228.1-2010	Round shoulders with 5-time cylindrical specimen	Le=30mm, d_0=6.02mm,
Gray cast iron	GB/T 228.1-2010	Round shoulders with 5-time cylindrical specimen	Le=30mm, d_0=6.01mm
Polypropylene (PP)	GB/T 1040.1-2010	Round shoulders with 5-time cylindrical specimen	Le=50mm, d_0=10.00mm

2. Equipments:

Table 3 Equipment information

Equipments	Manufacturer	Types
Field Emission Scanning Electron microscope	JEOL	JSM-7600F
Specimen Cutting Machine	BUEHLR	Delta AbrasiMet Cutter
Static Materials Testing Machine	Zwick Roell	Z100
Magnetron Sputter	SHINKKU VD	MSP-1S

3. Testing conditions:
Normal pressure and temperature

4. Procedure:
(1) Dog-bone specimen preparation: Prepare tensile specimens with two round shoulders with 5-time cylindrical specimen and a gauge in between by casting in a model with specific raw materials.
(2) Uniaxial tensile test: using vernier calliper to obtain diameters of cross section of specimens. Three points along the gauge range are picked, and at each point the measured value of diameter is the average of two results perpendicular to each other. Then, we load the specimen to the fixture at the proper position after setting primitive parameters.
(3) SEM specimen preparation: After fracture, fracture part of specimen are cut via wire cut electrical discharge machining and grind the surface slightly with abrasive papers. To enhance the conductivity of PP, fracture surface has to be sputtered with gold.
(4) SEM fracture morphology observation: Observe the microstructures of fracture morphology under the Field Emission Scanning electron microscopy (SEM) in various magnifications.

RESULTS AND DISCUSSION

1. Geometry parameters
Tab.4 shows the geometry parameters of specimen, d_0 is the primary diameter of specimen, S_0 is the cross-section area, L_e is the extensometer gauge length, d_f is the diameter of the specimen after fracture(we only measure d_f for ductile material, low carbon steel and PP)

Table 4 Geometry parameters of specimen

Specimen No.	Type	d_0 (mm)	S_0 (mm^2)	L_e (mm)	d_f (mm)
1	Low carbon steel	6.02	28.49	30.04	4.60
2	Gray cast iron	6.02	28.49	30.05	——
3	Polypropylene(PP)	10.00	78.54	50.05	9.50

2. Mechanical parameters
R_{eH} is the lower yield strength which approximately represents yield strength for ductile material, R_m is the tensile strength, $R_{p0.2}$ is the proof strength or offset yield strength which represents yield strength for no yielding materials(gray cast iron and PP, the machine also calculates the proof strength for low carbon steel, you can see that it is similar to lower yield strength) E is the Young's modulus, R_B represents fracture strength,
Based on GB/T 228-2010 "金属材料拉伸试验方法" and GB/T 1040-2010 "塑料拉伸试验方法", results should be rounded to the following precisions. For metal, strength values and modulus should in megapascals, to the nearest whole number; for polymer, strength value can round to 0.1Mpa, Young's modulus can round to 0.01GPa. (In principal, three valid numbers are needed for different materials)

Table 5 Mechanical parameters——strength and modulus

Specimen No.	E(GPa)	$R_{p0.2}$(MPa)	R_{eH}(MPa)	R_m(MPa)	R_B(MPa)
1	211	205	206	364	231
2	104	323	——	346	346
3	1.77	18.9	——	33.7	28.8

A_g is the percentage plastic extension at maximum force; A_{gt} is the percentage total extension at maximum force; A is the percentage plastic extension at fracture; A_t is the percentage total extension at fracture; Z is the percentage reduction of area.
Based on GB/T 228-2010 "金属材料拉伸试验方法"[3] and GB/T 1040-2010 "塑料拉伸试验方法"[4], results should be rounded to the following precisions. For ductile materials all other percentage extension and elongation values to the nearest 0.5 %; percentage reduction of area, Z, to the nearest 1 % (In principal, two valid numbers are needed for different materials)

$$Z = \frac{V_0 A}{A_0} \times 100\%$$

Table 6 Mechanical parameters——extension and reduction

Specimen No.	Ag	Agt	A	At	Z
	%	%	%	%	%
1	21.5	22.0	35.5	35.5	35
2	0.315	0.645	0.315	0.645	0.31
3	5.50	7.35	10.5	12.0	10

3. Stress-strain curve
Based on the extensometer, extension of gauge length is recorded and we can get engineering stress-strain curve for each specimen.(Shown in Fig.3)

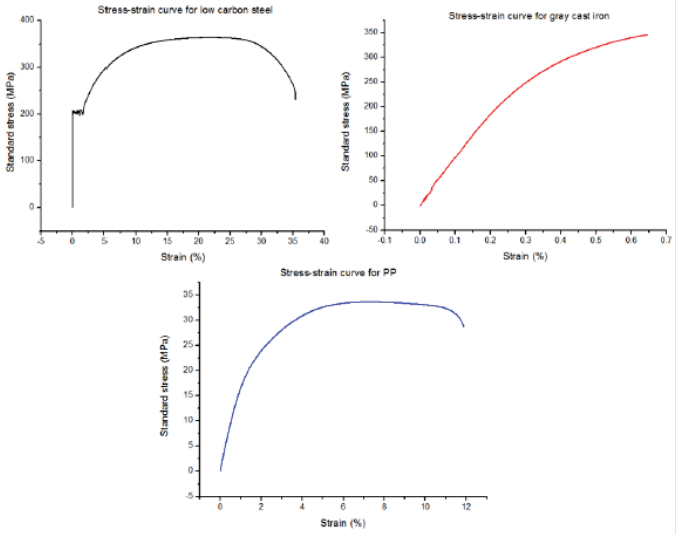

Figure 3 Stress-strain curve for each specimen

Based on stress-strain curve, we can see that for typical ductile material——lower carbon steel, four periods can be distinctly observed, first period is the elastic part, the strain is proportional to stress imposed in the specimen; second period, it get into yielding state, we can observe serrated stress-strain curve, which is largely caused by the Luders band, once the Luders band is overcome, you can clearly see the jerk stress-strain curve; third period is strengthening period, the stress will cause the motion of dislocation, since the interaction of dislocation will have the effect of cold strain hardening, the material is strengthened; and the

案例1 材料拉伸实验

fourth period, If the specimen is subjected to progressively increasing tensile force it reaches the ultimate tensile stress and then necking and elongation occur rapidly until fracture, we can judge necking by the increment of applied force equals to zero, after necking, plastic deformation is increased largely. During the experiment, we can see the shrinkage of the specimen in the middle part, and the speed of shrinkage is becoming faster and faster, when the cross-section area of specimen reached certain level, fracture happened, the applied load went down rapidly.

For gray cast iron, a quintessential brittle material, no four periods compared to low carbon steel. It can be approximately divide into two period, one is the linear elastic deformation part, the other is non-linear plastic deformation part. It does not have a yield point, and no strain-hardening. Therefore, the ultimate strength and breaking strength are the same. One of the characteristics of a brittle failure is that the two broken parts can be reassembled to produce the same shape as the original component as there will not be a neck formation like in the case of ductile materials.

For PP, it is only a ductile material since it has relatively large deformation prior to final fracture. However, subtle distinction compared to low carbon steel is that, there is no yielding period because there is no Luders band in polymer only polymer chain. The rest part is the same as low carbon steel, including elastic deformation part, strengthening part and necking, fracture.

To get a more transparent comparison of three different materials quantitively, we neglect the necking period of low carbon steel. (shown in Fig.4) And low carbon steel has a higher yield strength than PP, and so is Young's modulus. The results greatly depend on the interatomic bonding--metallic bonding is much stronger than intermolecular force. Whereas, brittle material has no obvious yield, stage of plastic deformation is very short and fractures at a tiny extension, because the cracks propagate so fast that the stress hasn't reached to its yield strength.

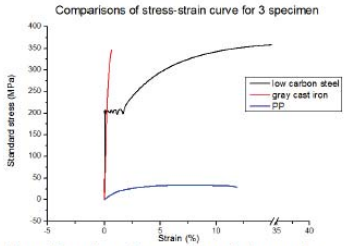

Figure 4 Comparisons of stress-strain curve for three specimen

4. Fracture morphology

For fracture morphology, we adopt SEM to characterize the fracture surface, we know that fracture morphology records all the information loyally from the initiation of crack to propagation of crack till final fracture. In that case, fracture morphology analysis can help us get access to more properties of materials.

4.1. Fracture morphology of PP

In the low magnification(×25,shown in Fig.5), the overall fracture morphology of polypropylene can be observed. Obvious distinction can be observed in radial direction, based on macroscopic fracture morphology, transitions from layer morphology to fiber morphology can be seen.AOI-a is the transgranular area which has a relative flat topography whereas AOI-b is the region which experience drastic tearing.

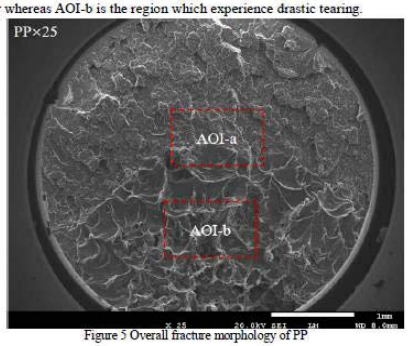

Figure 5 Overall fracture morphology of PP

To obtain better observation effect, we magnify each AOI with the magnification of 40, 200 and 1000.(Shown in Fig.6) to further judge the morphology of the fracture surface.

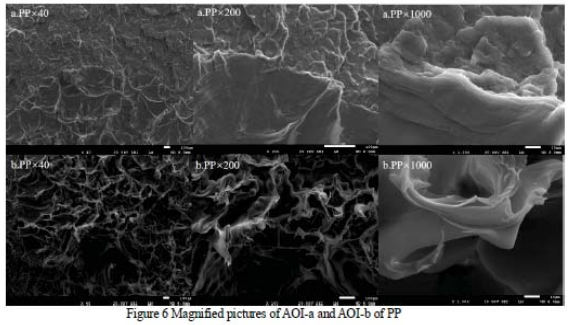

Figure 6 Magnified pictures of AOI-a and AOI-b of PP

For AOI-a, which is relatively far away from the source of fracture. Flat morphology is observed with several surface relief regions, polypropylene is a type of polymer which has multi-level interaction in a molecule. So the elongated layers fracture will be witnessed under low stress state. For AOI-b, which is just in the radial crack propagation ares, fibroid ribbon can be distinctly observed showing the acute tearing experience of materials, which means rapid propagation of crack happens here.

4.2. Fracture morphology of ductile and brittle metals

For overall morphology, we can evidently see that ductile material will have a cup-cone fracture(Fig.7 low carbon steel×25). We can see fibrous core and shear lip. Crack arises from the core fibrous region with no distinct crack source. For brittle material, no shrinkage of the surface, and uneven fracture surface is largely caused by rapid crack propagation and sudden fracture.

For low carbon steel, in the magnification of ×200 and ×1000, equiaxed dimple can be seen, especially, we can see several second phase particle in the dimple, which plays an significant role in fracture. During tension test, dimple or voids will coalesce to form a larger void giving rise to final fracture, the mechanism term is called micro-voids coalescence fracture.

However, for gray cast iron, tearing fibrous ribbon can be seen instead of dimple. In certain district, we cannot see tearing ribbon and the roughness of the surface is decreased (Fig.7 gray cast iron ×1000), it can conclude that uneven stress state is imposed in the specimen which mainly caused by heterogeneity of material. In the tensile test, the atom

案例1 材料拉伸实验

layer displacement will caused by uniaxial stress leading to final fracture. From mechanism aspect, we call it cleavage fracture.

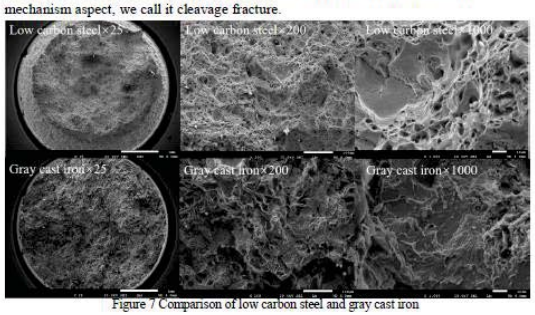

Figure 7 Comparison of low carbon steel and gray cast iron

Especially, we magnify shear lip in the magnification of ×40, ×200 and ×1000. With the expansion of the core micro-void and the reduction of necking region, crack will propagate rapidly. When crack is near the surface, the maximum shear stress will shear off the fracture surface in the direction of 45°, in that case, it will form a cup-cone fracture surface. Shots of shear lip can show us different morphology of specimens, we can evidently see slip of slip band in the direction of 45°. However, if we smooth the surface with special treatment, we may see more obvious slip phenomenon.

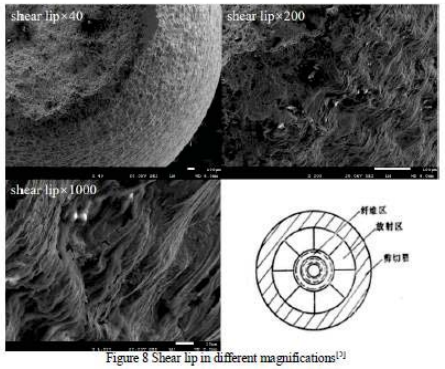

Figure 8 Shear lip in different magnifications[2]

CONCLUSIONS

1. From the tensile testing, stress-strain curve can be obtained. Low carbon steel and polypropylene have similar stress-strain curve as ductile materials, but jerk stress-strain curve in yielding caused by Luders band only happened in metal. For brittle material, gray cast iron, no distinct yielding period with only sudden fracture.
2. Related mechanical parameters are calculated automatically and manually. For different materials, they show completely different mechanical properties. In general, polypropylene has a lower strength and stiffness (Young's modulus).
3. Corresponding fracture morphology analysis is carried out via SEM, polypropylene fracture surface shows relative flat surface and drastic tearing ribbon morphology which represent slow propagation and rapid propagation region of crack. Low carbon steel has a cup-cone fracture with fibrous region and shear lip, its fracture mechanism is micro-voids coalescence fracture since massive dimples are observed. Gray cast iron has an uneven surface caused by cleavage fracture.

REFERENCE

[1] William D. Callister, Jr. Fundamentals of Materials Science and Engineering [M]. the USA: Von Hofmann Press, 8th Edition, 2015:234-240.
[2] Lecture notes on mechanical properties by LT Kong.(Last updated: Feb 23, 2016)
[3] GB/T 228.1-2010 金属材料拉伸试验方法
[4] GB/T 1040.1-2010 塑料拉伸试验方法
[5] 张帆，郭益平，周伟敏. 材料性能学（第二版）[M]. 上海：上海交通大学出版社，2014

ACKNOWLEDGEMENTS

We would like to express our heartfelt thankfulness to Prof. Wu and Prof. Zhou to provide elaborate instructions during the experiment. And we would like to thank TA for provide guidance for SEM observation. Last but not least, I would thank my group members.

案例2 盐类结晶实验（18级）

上海交通大學
SHANGHAI JIAO TONG UNIVERSITY

Ionic Compound Crystallization

Materials Science and Engineering

Course No. MT344

Guided by Prof. Weimin Zhou and Prof. Xueyan Wu

Written by

Rouyan Guo 郭若岩 518021910569
Kesen Wang 王可森 518051910034
Ce Xu 徐 策 518051910036
Han Wang 王 涵 518021910502
Runhua Li 李润华 518021911136

2020/12/12

TABLE OF CONTENTS

1. INTRODUCTION

Crystallization is the process with long range order solids formation (known as crystal). This phenomenon can be observed in many minerals in nature. The minerals appear to have reproducible structure and the surfaces intersect with certain angles as shown in Figure 1. The application of crystallization in industry ranges from the isolation of the few mg illigrams of a substance newly synthesized in the laboratory – where a well-defined melting point is used to both achieve and prove a decent purity of the crop and as an identity check – to a mass crystallization carried out in very diverse industries.[1]

Figure 1. Morphology of quartz mineral.[2]

The crystal forms usually by means of precipitating from a solution or freezing from liquid phase. A few methods of deposition directly from gaseous phase are proposed and applied in crystallization as well. A typical crystallization of salt from supersaturate solution includes two stages: nucleation and growth. Only when the clusters in solution reaches the critical size then a stable nuclei can be formed. By continuous cooling to room temperature, the nuclei size grows and precipitate. This process is affected by many internal and external factors, for instance, solubility of material, the composition of solution, temperature, pressure, etc.

In this work, we prepare the solution of copper sulfate ($CuSO_4$) and ammonium chloride (NH_4Cl) respectively and heated to 70°C, then the solution crystallized by natural cooling. The crystallization process is observed under a microscope. The crystallization feature of two ionic compounds are discussed and the understanding of crystallization laws are emphasize.

案例2 盐类结晶实验

2. THEORY

2.1 Crystallization kinetics

2.1.1 Nucleation

For the nucleation, different processes have to be distinguished (**Figure 2**). Spontaneous nucleation can occur either in the absence of any foreign surface, the so-called homogeneous nucleation, or on foreign surfaces such as dust, the so-called heterogeneous nucleation. This type of nucleation is also called primary nucleation, and is distinct from secondary nucleation, where the generation of new particles is induced by particles of the solute.

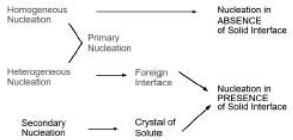

Figure 2. Different kinds of nucleation.

The mechanisms of primary nucleation can best be discussed by using the nucleation of droplets from the vapor phase. Using droplets instead of crystals, the treatment of polyhedral bodies and the differences in interfacial tension of individual faces can be avoided, making the understanding of the treatment easier. The principles can be transferred to polyhedral crystals.

To derive the nucleation rate, the free enthalpy of the formation of a droplet with a radius r, $\Delta_r G$, has to be calculated (**Figure 3**). Two terms contribute to the free enthalpy – the enthalpy of condensation and the enthalpy necessary for creating the new surface (**Equation 1**):

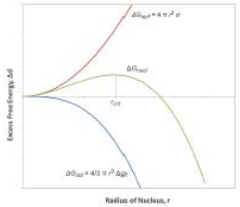

Figure 3. Nucleation of a droplet with size r from a supersaturated vapor phase. [1]

$$\Delta_r G = \frac{4\pi}{3} r^3 \Delta_v G + 4\pi r^2 \sigma \qquad (1)$$

The enthalpy of condensation ΔG per volume of a building block is given by

$$\Delta G = (RT/\Omega) \ln(p/p_\infty) = (RT/\Omega) \ln \beta \qquad (2)$$

With Ω as the molar volume. The enthalpy for creation of the new interface is given by the surface area of the droplet and the surface tension σ.

For a droplet to grow, the change in free enthalpy upon adding a building block has to be negative. It is apparent from **Figure 3** that this is the case only for $r > r^*$. For droplets with a size $r < r^*$, the addition of a building block is unfavorable, as the free enthalpy increases. Thus, a droplet with a size of $r = r^*$ has the same probability of adding a growth unit as losing it; it is in equilibrium with the supersaturated mother phase.

The nucleation rate J is given by the density of the nuclei multiply the rate of addition of one further building block. The volume density of critical nuclei can be derived using the Boltzmann equation, which relates the concentration of oligomers n_i to the concentration of monomers n_1, to the free enthalpy for the aggregation:

$$n_i / n_1 = \exp(-\Delta G / RT) \qquad (3)$$

From **Equation 1, 2**, the size of the critical nucleus, r^*, can be derived (**Equation 4**):

$$r^* = \frac{2\sigma}{\ln \beta} \cdot \frac{\Omega}{RT} \qquad (4)$$

Thus, the free enthalpy to form such a critical nucleus, the enthalpy of nucleation, is given by:

$$\Delta_r G^* = \frac{16\pi}{3} \sigma^3 \frac{1}{\Delta_v G^2} = \frac{16\pi}{3} \sigma^3 \left(\frac{1}{(RT/\Omega) \ln \beta} \right)^2 \qquad (5)$$

The dependence of building block addition rate on supersaturation can be neglected. Since the formation free enthalpy is proportional to $(1/\ln\beta)^2$, thus the nucleation rate depends exponentially on supersaturation, as given by **Equation 6**:

$$J = k' \cdot \exp\left(-\frac{\Delta_r G^*}{RT}\right) \qquad (6)$$

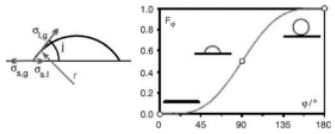

Figure 4. Correction factor F_φ for the nucleation of a droplet on a flat surface as a function of the contact angle φ. [1]

Nucleation can also occur on the surface of a foreign particle. The free enthalpy of the formation of a droplet on a surface is decreased. A factor F_φ relates the free enthalpy of nucleation on a surface $\Delta_r G^*$ to that in the volume (**Equation 7**). For a flat surface, the qualitative dependence of F_φ on the contact angle is shown in **Figure 4**. For a contact angle of $\varphi = 180°$, the liquid will not spread and the foreign surface does not support the nucleation; conversely, for $\varphi = 0°$, the liquid spreads on the surface and no barrier to nucleation has to be overcome.

$$\Delta_r G^* = F_\varphi \Delta_{r,0} G^* \qquad (7)$$

As the factor is always smaller than unity (except for $\varphi = 180°$), the nucleation on a surface is energetically favorable to homogeneous nucleation, and will thus have drastically higher rates.

案例2 盐类结晶实验

2.1.2 Growth

Steps on ideal crystals can be formed by 2D nuclei. As discussed before, the supersaturation necessary for nucleation on a surface is significantly lower than the supersaturation necessary for nucleation in the volume.

Due to the limit time, of the three models for the growth via 2D nucleation, we only discuss birth-and-spread model will here. In this model, 2D surface nuclei are generated on the flat faces. The nuclei are limited by steps that will spread out. It is allowed that new nuclei generate on growing islands (**Figure 5**).

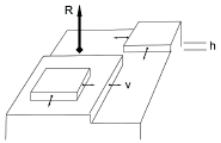

Figure 5. Model for the growth via 2D surface nuclei according to the birth-and-spread model. [11]

The growth rate of the nuclei depends exponentially on supersaturation (**Equation 8**):

$$R \propto e^{-\frac{\Delta G^*}{RT}} \quad (8)$$

Thus, the growth via 2D nucleation will need a certain critical supersaturation to start, upon which the growth rate will increase rapidly, until it is limited by transport phenomena.

Besides being determined by processes at the interface of a crystal, the growth rate can also be determined by transport phenomena in the bulk of the mother phase. In the case of growth from solution, the discussion of transport phenomena can be limited to the transfer of mass.

The diffusion layer in a stagnant solution has a thickness of approximately 1 mm. The mass transfer by diffusion equals the mass transfer by incorporation of building blocks into the crystal by interfacial processes. Two regimes can be distinguished, growth mainly determined by diffusion and growth mainly determined by the processes at the interface.

2.2 Affecting factors

2.2.1 Usual thermodynamic variables

Crystallization is governed by the usual thermodynamic variables of temperature, composition, and pressure. It is common to describe the thermodynamics in terms of dominant chemical species present, which in the majority of crystallization processes are the material to be crystallized and a small number of solvents.

Supersaturation is one of the important affecting factors. The supersaturation is mainly controlled by temperature. The lower the temperature, the lower the supersaturation. The larger the supersaturation is, the more nuclei are produced and the smaller the grain size is.

The crystallization time is also an important affecting factor. It is related to the height of liquid. The higher the liquid is, the longer the crystallization time is. The longer the crystallization time, the larger the grain size of the crystals.

Stirring intensity is another affecting factor. The stronger the stirring, the more easily the crystal is broken. And the crystal particle size will be smaller.

2.2.2 Additives and impurities

For all real systems, a further influence has to be taken into account, that is, of impurities. These are present in every system, in varying amounts. These impurities can have an effect on the solubility or melting point of the material to be crystallized, if small. The presence of additional components in the solution is often more noticeable in their effect upon the kinetics of crystallization and more specifically on growth rates of crystals.

(a) Solubility

As the solubility of a given substance in a given solvent depends upon the composition of the system, the solubility will change with the presence of additional chemical species. Currently, it is not possible to predict the precise effect an additional component will have, but experience shows that the solubility of a substance generally increases in the presence of additives.

One exception is the so-called common ion effect observed in electrolyte solutions. Here, the solubility product governs the solubility behavior (**Equations 9**):

$$A_\nu B_\mu \rightleftharpoons \nu A + \mu B$$
$$K_s = [A]^\nu [B]^\mu \quad (9)$$

The presence of a second electrolyte sharing a common ion with the dominant species will reduce the solubility. The solubility product K_s is a constant, and any increase in the concentration of one or the other

component reduces the concentration of the counterion. As a result, the apparent solubility of the salt is decreasing.

(b) Nucleation rates

The presence of foreign species in a solution may increase or decrease the nucleation rate of the crystallizing substance. Both effects can be understood in terms of classical nucleation theory, where the nucleation rate is given by

$$J = J_0 e^{-\left(\frac{B\gamma_{sl}^3 v_m^2}{(kT)^3 (\ln S)^2}\right)} \quad (12)$$

J_0 is a pre-exponential factor, the shape factor C_B accounts for the geometry of the nucleus, γ_{sl} is the interfacial energy of the nucleus with respect to the solvent, V_{mol} is the molecular volume, k the Boltzmann constant, T is the temperature, and S is the relative supersaturation. The presence of additives may increase or decrease the interfacial energy, which will result in a respective increase or decrease of the nucleation rate.

Additives may also affect the equilibrium solubility of a solute and thereby modify the supersaturation, which in turn results in a change in nucleation rate.

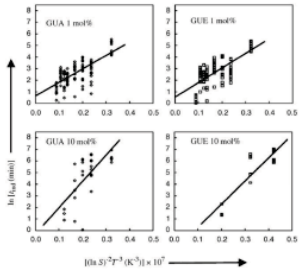

Figure 6. Data of the induction time for the nucleation of vanillin in 2-propanol/water in the presence of various additives and regressions. [11]

This is illustrated in **Figure 6** for the induction time of the nucleation for vanillin in 2-propanol/water in the presence of various additives.

案例2 盐类结晶实验

By the way, additives may also affect the equilibrium solubility of a solute and thereby modify the supersaturation, which in turn results in a change in nucleation rate have a growth rate-modifying impact and, as a consequence, morphological changes of the crystals are observed. **Figure 7** presents the corresponding effect on the normalized growth rates of calcium oxalate monohydrate (COM) in the presence of citrate and the morphological changes.

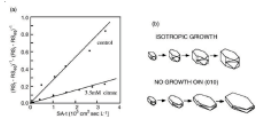

Figure 7. (a) Determination of the crystal growth rates of COM crystals: reference and reduced growth rates in the presence of citrate. (b) Isotropic growth of the control sample (top) and inhibited growth in the presence of citrate (bottom).[11]

3. MATERIALS AND METHOD

3.1 Materials and equipment

(1) Petri dishes, beakers, test tubes, ammonium chloride powder and copper sulfate powder

(2) Prepared aqueous solution with a mass fraction of 25%~30% ammonium chloride

(3) Prepared copper sulfate aqueous solution

(4) Electric-heated thermostatic water bath in **Figure 8** and thermometer

Figure 8. Electric-heated thermostatic water bath.

(5) Biological microscope

Figure 9. Biological microscope.

3.2 Procedures

(1) Prepare aqueous solution with a mass fraction of 25%~30% ammonium chloride.

(2) Put the solution into a beaker and heat it in the electric furnace to near 70 °C.

(3) When the temperature of solution reaches stable, take the solution with a dropper and drop one drop onto the petri dish.

(4) Observe the crystallization of ammonium chloride under biological microscope and take pictures during this process.

(5) Prepare the copper sulfate aqueous solution and repeat the above procedures.

4. RESULTS AND DISCUSSIONS

4.1 Crystallization of ammonium chloride

The crystallization process is observed under the biological microscope and the overall process is roughly shown in **Figure 10**.

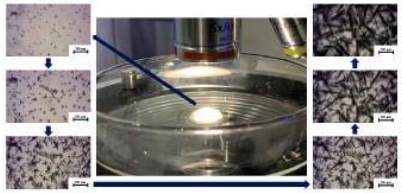

Figure 10. Crystallization process of ammonium chloride.

By observing the crystallization process, we can see that the crystal is firstly formed at the bottom of beaker for the reason that the bottom of beaker locates the nearest to the external environment and therefore, the highest temperature difference acts as a driving force for crystal to nucleate and grow. **Figure 11** exhibits the initial nucleation and growth of crystals. Besides, the crystals drift in the way of Brownian motion.

案例2 盐类结晶实验

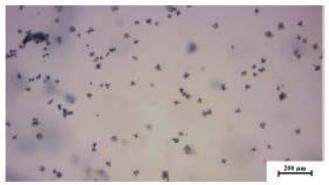

Figure 11. Initial nucleation and growth.

In the first stage, the small crystals grow separately and their growth rate is obviously different from each other. Some ammonium chloride crystals grow individually while some grow as a cluster. In **Figure 12**, we can see that dendrites grow on the original crystal and the number of dendrites on most crystals ranges from four to six. The shape of most crystals is irregular octahedron since different dendrites also have different growth rates.

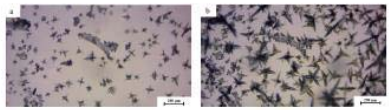

Figure 12. The first stage of ammonium chloride crystallization.

The amount of crystals at the bottom of beaker increases in the second stage and the secondary dendrites grow on the surface of primary dendrites. The bottom of solution is gradually filled with crystals, after which the crystals begin to grow on the upper layer of solution. The growing process is similar to that on the bottom layer.

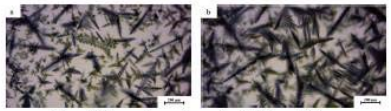

Figure 13. The second stage of ammonium chloride crystallization.

In the final stage, the bottom and upper layers are filled with crystals and the tertiary dendrites grow on the secondary dendrites. Compared to the primary dendrites, the size of secondary dendrites is much smaller than that of primary dendrites. Likewise, the size of tertiary dendrites is smaller than that of secondary dendrite and therefore, it is quite difficult to observe its appearance under the biological microscope. As time goes on, the crystallization process comes to an end and the final circumstance is shown in **Figure 14**, which is covered by many grown crystals at different depth.

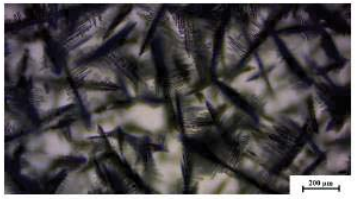

Figure 14. The finish of ammonium chloride crystallization.

4.2 Crystallization of copper sulfate

4.2.1 Crystal Morphology Analysis

Copper sulfate has a triclinic lattice with a=0.586nm, b=0.612nm, c=1.072nm and α=77.42°, β=82.41°, γ=72.74° (see **Figure 15a**). Therefore, when precipitating from water, the crystal tends to appear in irregular prisms. Different surfaces of the prism are related to different lattice planes, as showed in **Figure 15b**.

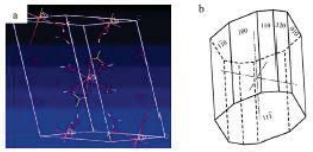

Figure 15. Lattice of copper sulfate.[11]

Pictures of the crystallization process are selected to research certain terms of the crystallization of copper sulfate.

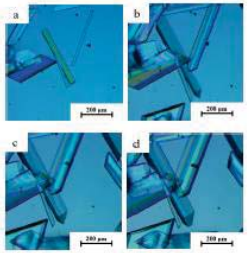

Figure 16. Crystallization of copper sulfate.

In **Figure 16a**, new crystal forms in a rectangular shape with some high-energy lattice plane exposed in the solution. In **Figure 16b**, to reduce the total free energy, new surfaces with lower energy level are formed. **Figure 16c** clearly shows a new layer growing on the former crystal surface, which is consistent to the 2D nucleation and growth theory. This mechanism provides much more convenience for crystal to expand. The final shape of the crystal is showed in **Figure 16d**.

4.2.2 Crystallization Kinetics Analysis

In order to better study the process of crystallization, we can measure the width and length of the crystal separately. Supposing the width and length is measured at d and l, we may estimate the volume of the crystal $V=kd^2l$. Relating the volume of the crystal with time, we can mathematically analyze the process of crystallization.

From the video recorded during the experiment, the data are collected and fitted into a curve of polynomial function (**Figure 17**).

案例2 盐类结晶实验

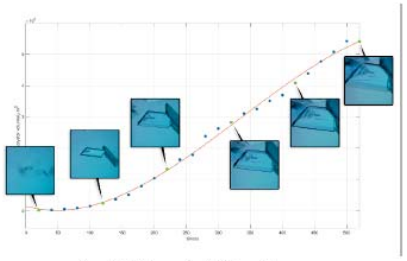

Figure 17. Fitted curve of crystal volume and time.

Table 1. Specific fitting terms

Fitting Function	a	b	c	d	R^2
f(x)=ax³+bx²+cx+d	-0.6282	629.8	-56560	1.505000	0.9958

According to the fitting result, we can also work out the differential curve of the Vt function, which indicates the relationship between crystallization rate and time, and the result is in parabola shape (**Figure 18**).

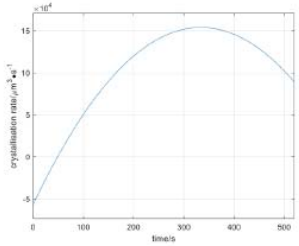

Figure 18. The curve of crystallization rate.

Given the parabola shape of the curve, it is obvious that the growth rate of the crystal will first increase and then decline. This phenomenon can be explained by the following reasons:

(1) At first, there is no under-cooling in the solution, and the driving force of nucleation is low. Thus, though growth is highly activated, the crystallization rate is low.

(2) After some time, the under-cooling reaches certain extent, the condition is suitable for both nucleation and growth, the crystallization rate achieve its maximum.

(3) Along with the falling temperature, the driving force of growth becomes the dominant limitation for the crystallization process, and the rate begins to decrease.

(4) As the crystallization goes on, the concentration of copper sulfate also decreases, which contributes to the reduction of crystallization rate.

5. CONCLUSIONS

In this work, we prepare the solution of copper sulfate ($CuSO_4$) and ammonium chloride (NH_4Cl) respectively and heated to 70° C , then the solution crystallized by natural cooling. We found that the crystallization of NH_4Cl follows a multistage process, the primary dendrites grows with a shape of irregular octahedron, followed by the growth of smaller second dendrites on the primary dendrites. Through the observation of $CuSO_4$ crystallization, we notice that the crystals of $CuSO_4$ tend to appear in irregular prisms. To better study the crystallization kinetics of $CuSO_4$, we analyze the volume change of the crystal versus time and calculate the dynamic crystallization rate during the whole process. We also provide reasonable explanation of the result we find.

REFERENCES

[1] Crystallization: basic concepts and industrial applications [M]. John Wiley & Sons, 2013.

[2] FossilEra. (2020). FossilEra :About Minerals & Crystals. Retrieved from https://www.fossilera.com/pages/About-minerals-crystals

[3] Polymer Science. (2020). Polymer Property Database : THERMODYNAMICS OF HOMOGENEOUS NUCLEATION. Retrieve difrom https://polymerdatabase.com/polymer%20physics/Spherulites.html

[4] Justel FJ, Camacho DM, Taboada ME, Roberts KJ. Crystallisation of copper sulphate pentahydrate from aqueous solution in absence and presence of sodium chloride. J Cryst Growth. 2019;525.

案例3“铝硅铸造合金的组织和性能”汇报视频部分

学生收获-摘自17年首届学生汇报

Review | Result | Defect | Future

Reports writing

Doing report is what we learned in this semester, and there are so many tips to make sure the reports meet demands.

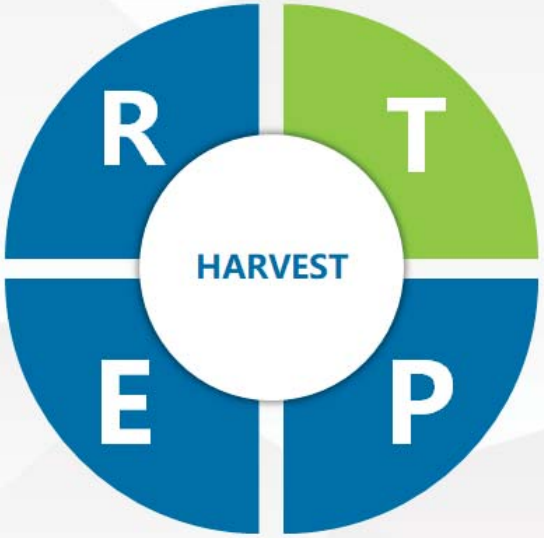

Theory learning

During doing the report, theory parts help me to comprehend the concepts.

Experimental techniques

Techniques for experiment are trained, and it is of importance to have a try on basic experiments.

Presentation skills

It is obvious that presentation can enhance understanding of what we learn and train our oral expression skills.

学生收获-摘自17年首届学生汇报

2. My gains and advice——gains

(1) Basic knowledge of macro properties and micro structure of materials, better understanding of theory.

(2) Ability to write a standardized experiment report.

(3) Better proficiency in certain software.

(4) Ability to have group cooperation and confidence to do the presentation

(5) Exciting and interesting stories from Zhou

Patient and helpful guidance from Wu

Careful and thorough evaluation from Chen

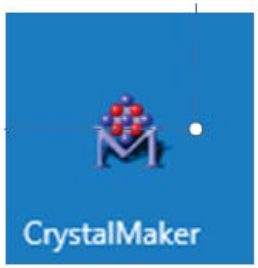

学生收获-摘自19年学生汇报

学生收获-摘自19年学生汇报

MY GAIN

It transformes the abstract theoretical knowledge into practical material behaviors.

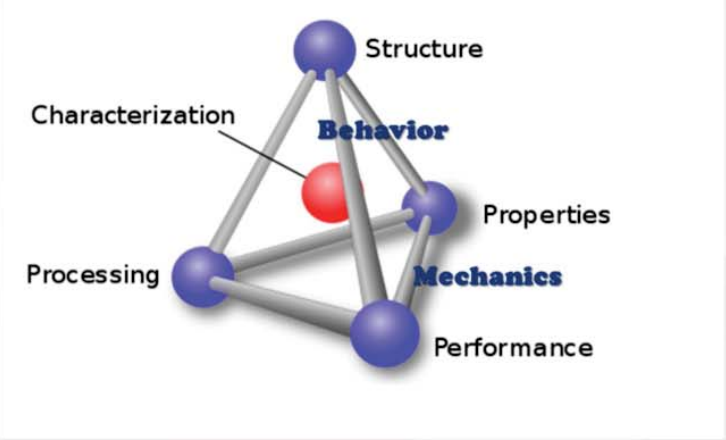

- Useful Testing Methods
- Intuitive material properties
- Deeper understanding of materials
- Good atmosphere and interesting experience

反思

实验教学英语讲课的利与弊

5届学生的变化：首届学生不爱写报告，本届学生过度注重报告的分数

对金相实验的再认识

历届参与金相大赛的选手去向

年份	届数	学生去向
12	1	赴美读博 交大博士 交大博士
13	2	交大硕士 交大硕士 新加坡南洋理工硕士
14	3	
15	4	交大和法国双硕士 交大硕士 美国俄亥俄州立大学
16	5	江苏选调生） 交大硕士 交大硕士
17	6	交大硕士 国际班，交大致远荣誉博士） 澳洲硕士
18	7	国际班，推免北大硕士 推免交大直博 推免交大直博
19	8	国际班推免交大硕士、 国际班

01 材料实验教学中心概况

02 国际化实验教学介绍

03 赛事展望

一个精彩的赛事，值得期待

材料学院有丰富的举办大型活动的能力

去年10月材料学院举办的材料日活动

闵行校区位于上海西南


距离市中心人民广场30公里
距离浦东国际机场49公里，驾车约44分钟，车费约130元
距离虹桥国际机场（火车站）约29公里，驾车约30分钟，
公共交通：校区西部有5号线，东部有新开通的15号线
上海市
虹口区
黄浦江
内环共和新路立交桥
外环高速
普洛斯合庆物流园
环东二大道立交
海棠公园
中山公园
世纪公园
东岸绿道
纪王公园
沪杭铁路立交桥
外环北翟路立交桥
上海虹桥国际机场
新虹桥中心花园
南园滨江绿地
华夏高架路
华夏公园
迎宾立交桥
中环路
上海龙华古寺
上海浦东国际机场
上海绕城高速
沪常高速
纪鹤公路
老油车港桥
博园路
博览公园
两岸浦
香花立交
郑一工业区
青浦区
青松路跨线桥
上海政法学院
辰山植物园
广富林文化遗址
昆秀湖湿地公园
松江中央公园
大港立交
松江区行政服务中心
方塔园
松江南站
松蒸公路
沪昆高速立交桥
新五厍镇
双汇村
陈阁
竹三里
叶榭站
车墩站
古藤园
韩湘水博园
北松公路
旗忠网球中心
上海交通大学（闵行校区）
放鹤路
上海浦江郊野公园
沪闵公路
沪松公路
沈海高速
虹梅南路
龙吴路
林海公路立交桥
申嘉湖高速
五灶港桥
坦直镇
上海健康医学院南宛
上海交通职业技术学院(浦东校院)
南汇桃花村
浦东上海绕城高速立交桥
沪南公路
两港公路
浦星公路
洪桥景区
大叶公路
南张
三墩镇
大治河
东征村
东现村
滨海世外桃源
上海滨海森林公园
上海鲜花港
三团港
万四村
周家圈
华田泾
岛旅游假区
明星

闵行校区占地近5千亩，有校内巴士

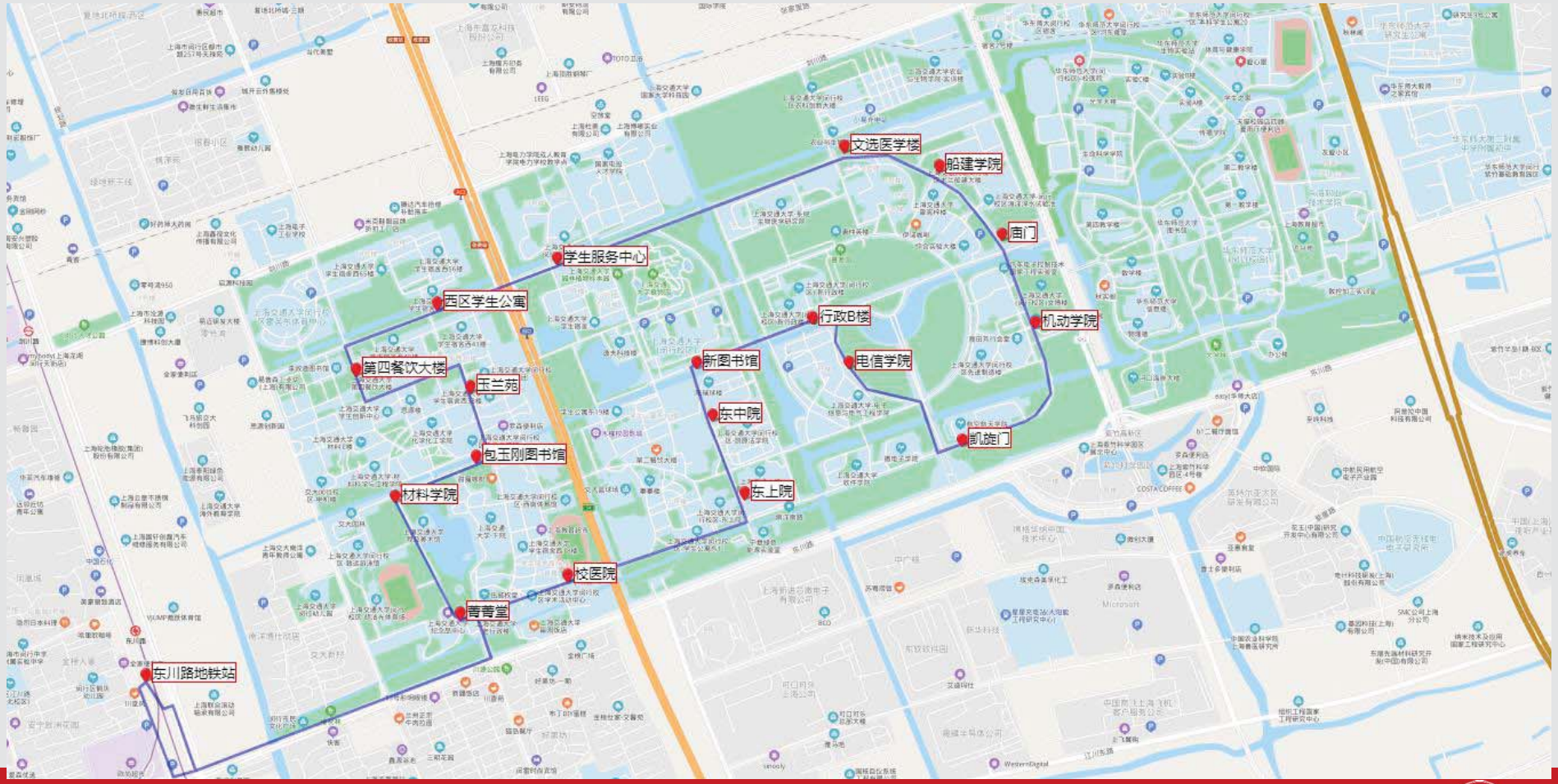

结束语

热烈欢迎全国兄弟院校相聚东海之滨、相会思源湖畔！

热切期盼第十届全国大学生金相技能大赛成功举办！

上海交通大學

SHANGHAI JIAO TONG UNIVERSITY

Thank you!